Initialization Shock in CCSM4 Decadal Prediction Experiments

Haiyan Teng, Gerald A. Meehl, Grant Branstator, Stephen Yeager, Alicia Karspeck

National Center for Atmospheric Research, Boulder, USA

Introduction

Initialized predictions tend to drift away from the initial states towards the model's imperfect climatology. If all predictions drift in a coherent manner that is independent of an initial state, the drift to a large extent can be removed during the posterior bias correction. However, lack of continuous global ocean observations poses a serious challenge to the quality of ocean initial states that span several decades. Furthermore, incoherent initial errors especially in the Tropics can be amplified by air-sea coupling as a prediction evolves and can impact the entire globe through atmospheric teleconnections. Consequently the effect of such initial shocks on predictions are difficult to remove by simple bias correction methods and can overwhelm the relatively small decadal signals that we seek to predict. Here, we describe the initialization shock in a set of decadal prediction experiments with the Community Climate System Model version 4 (CCSM4) and discuss the challenges they cause to near-term hindcasts, in particular of the Interdecadal Pacific Oscillation (IPO).

CCSM4 decadal prediction experiments

CCSM4 is a fully coupled general circulation model consisting of atmosphere, ocean, land, and sea ice that are linked via a flux coupler and no flux corrections are employed (Gent et al., 2011). The atmosphere model uses a finite volume dynamical core with a nominal horizontal resolution of 1°and 26 layers in the vertical. The ocean is a version of the Parallel Ocean Program (POP) with a nominal latitude-longitude resolution of 1° (tapering down to 1/4° in latitude in the equatorial tropics) and 60 levels in the vertical. The land and sea ice components share the same horizontal grids as the atmosphere and ocean models, respectively.

The CCSM4 decadal prediction experiments (also referred to as initialized hindcasts, or hindcasts) analyzed here are an expansion of a previously documented set (Yeager et al., 2012) that was submitted to the Coupled Model Intercomparison Project phase 5 (CMIP5) (Taylor et al., 2012). The ocean/sea ice initial conditions are obtained from a CCSM4 ocean/sea ice stand-alone simulation forced with atmospheric variables, such as surface winds, air temperature, precipitation, surface fluxes, sea level pressure, humidity etc. from the NCEP/NCAR reanalysis

(Kalnay et al., 1996). This forced ocean/ice simulation represents the NCAR contribution to the

Coordinated Ocean-ice Reference Experiments phase II (CORE II) (Danabasoglu et al., 2014). The initial states for atmosphere/land are taken from CCSM4 CMIP5 uninitialized historical/RCP4.5 runs. For each January 1st during 1955-2014, we ran a 10-member ensemble of initialized hindcast experiments with the ensemble spread created by perturbing the atmosphere (or both atmosphere and land in the earlier set as documented by Yeager et al., 2012) initial conditions.

There exists a large variety of bias correction methods and they are designed to reduce errors and add skills to the forecasts. To avoid complexities that can arise in assessing the source of improvements in calibrated initialized hindcasts compared to the traditional climate change projection experiments without initialization (also referred to as the uninitialized simulations), here we examine interannual anomalies with respect to a hindcast climatology that is only a function of prediction range; no observations are taken into account in our calculation of anomalies (as in Doblas-Reyes et al., 2013). That is, at lead t (t=Month1, 2, …, 120) from a start year j (j=year 1955, …, 2014), the interannual anomalies

$$Y'_{jt} = Y_{jt} - \sum_{k=1}^{N} Y_{kt}/N, \qquad (1)$$

where Y_{jt} is the raw hindcast, and N is the total number of start years. By using this methodology, the reference model hindcast climatology $\sum_{k=1}^{N} Y_{kt}/N$ already includes most model systematic errors (including systemic errors in the forced response, assuming the forced response is independent to the initial states). Presuming initial errors are the same for different start years, computing differences on the right hand side of (1) will leave mostly the signal in the hindcasts. A caveat is that the initial errors often vary with start years, which is even more true for decadal predictions than for seasonal predictions, as the former covers decades with limited ocean observations.

Warm shocks in the Nino3.4 SST

First, we focus on sea surface temperature (SST) in the Nino3.4 region for the hindcast behavior. Fig. 1a shows the time evolution of raw Nino3.4 SST during the 10-year

hindcast period; with each colored thin line representing a raw 10-member ensemble mean hindcast from a start year indicated by the label bar, and the thick black line representing the observed climatology (http://www. esrl.noaa.gov/psd/gcos_wgsp/Timeseries/Data/nino34. long.data). Strikingly, the Nino3.4 SSTs from hindcasts initialized during the early decades (1955-1970, dark blue) tend to produce a 2°C warm spike relative to the observed climatology in the first two or three years. By contrast there are no obvious warm spikes in the later start years, and a number of hindcasts initialized around year 2000 produce cold spikes of roughly -2°C in the first three years.

We further examine the hindcasts of Nino3.4 SST at three different lead times by comparing predicted interannual anomalies defined by (1) to observed anomalies derived by subtracting the observed climatological mean. In Month1 (Fig.1b), the hindcast anomalies (red) generally match the observations (black). This reflects the consistency of the initial states with the observations. Because we cannot effectively remove the initial shock that is most pronounced in Year 2 with the calculation in (1), the Year 2 annual mean Nino3.4 SST hindcast anomalies show a pronounced multidecadal shift, with more than 1°C anomalies in the early two decades and -1°C anomalies in late 1990s and the early 2000s (Fig. 1c). The observed anomalies do not have these multidecadal variations suggesting that the variations are examples of impacts from initialization shocks that cannot be removed by simple bias correction techniques.
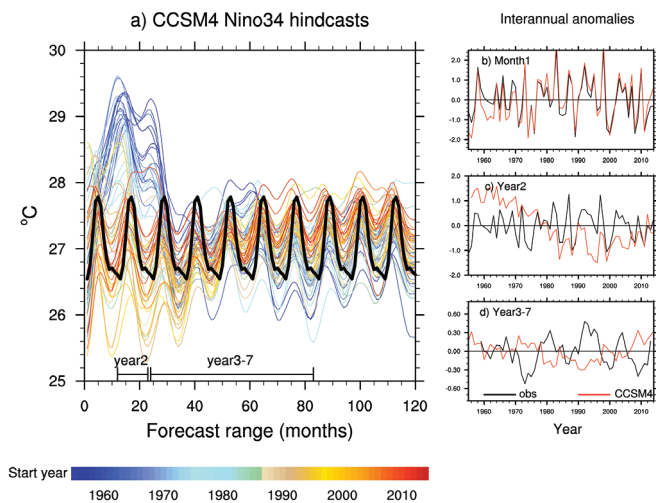
Year 3-7 is the forecast range that some current decadal prediction experiments aim to target (Meehl et al., 2014a, 2014b, 2016; Meehl and Teng, 2012, 2014a, 2014b). The tropical Pacific, which is a pace-maker of global climate (Kosaka and Xie, 2013), has limited initial-value predictability for all initial states at this range of 3-7 years based on a "perfect model" assessment (Branstator and Teng, 2010). When we calculate the Nino3.4 SST interannual anomalies at the Year 3-7 range (Fig.1d), we still find secular multidecadal variability, with a downward trend until about 1980, and then stable or somewhat upward after that. In some ways this is reminiscent of the Year 2 drifts (Fig. 1c). Note there is a change in the range of the y-axis from Fig.1bc to Fig.1d; the amplitude of the Year 3-7 anomalies is much weaker.

What caused the shock?
First, we examine how closely the ocean initial conditions reflect observations by comparing the Month1 hindcasts and the corresponding January observations. We focus on SST and subsurface temperature measured by the thermocline depth (20°C isotherm, Z20) in the equatorial Pacific, with the observed SST obtained from HadISST (Rayner et al., 2003) and the Z20 observations calculated from the 2009 World Ocean Database (Levitus et al., 2009). Our main focus is not climatological meanbiases but a possible change in either the strength or distribution of the initial errors occurring at about 1980 that might explain why the positive initial shock only occurs for start years between roughly 1955-1970.
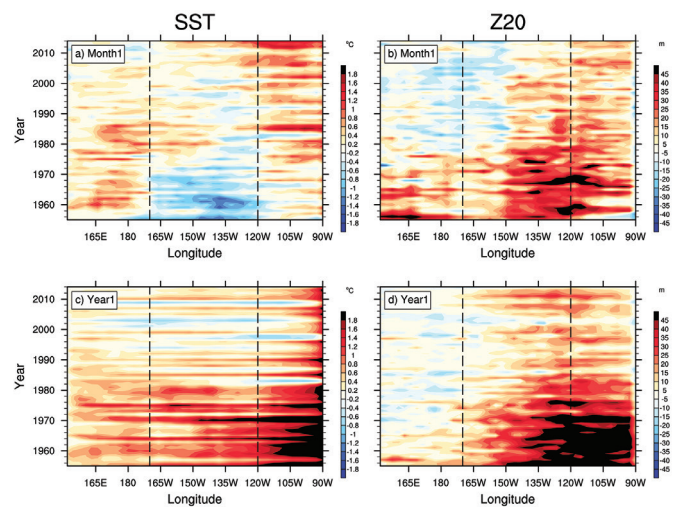

Figure 1: (a) Time evolution of raw Nino3.4 SST during the 10-year hindcast period, with each colored thin line representing a 10-member ensemble mean hindcast from a start year indicated by the label bar, and the thick black line representing the observed climatology. The hindcast SSTs are smoothed by an unweighted 6-month running average. b-d) interannual Nino3.4 SST anomalies from the CCSM4 hindcasts (red) and observations (black) at three different forecast ranges: **(b)** Month 1, **(c)** Year 2 and **(d)** Year 3-7.

Figure 2: Start year vs. longitude distribution of Month1 (top) and Year1 (bottom) errors in equatorial SST (5°S-5°N) and 20°C isotherm depth (Z20, 2°S-2°N). Boundaries for the Nino3.4 region are outlined by the two vertical dashed lines. The observed SST and Z20 are obtained from HadISST (Rayner et al. 2003) and 2009 World Ocean Database.

The warm spikes in the Nino3.4 region in the early hindcast period do not seem to be directly caused in any obvious way by the SST initial errors, for those initial errors are generally negative ($\sim$ -1°C) during 1950-1970 and are actually cooler than the errors in start years after 1980 (Fig. 2a). However, the Z20 errors are much deeper in the pre-1980 initial conditions compared with the later period (Fig. 2b), indicating that the early start years have a much warmer subsurface temperature bias (hence deeper Z20). This subsurface warm bias is further amplified during Year 1 (Fig. 2d) and appears to have propagated to the surface (Fig. 2c).

We further diagnose the interannual temperature tendency budget in the upper 100m in the Nino3.4 region:

$$\frac{\partial T'}{\partial t} = -\frac{Q'_{net}}{\rho_0 C_p H} + UET'_{W-E} + VNT'_{S-N} + WTT'_{100m} + residual \quad (2)$$

where T is the depth averaged temperature anomaly, Q_{net} is the net air-sea surface flux. H, ρ_0, and C_p are three constants that denote the layer thickness (=100m, and consistent results are found for H=60m), water density, and heat capacity, respectively. UET_{W-E} and VNT_{S-N} denote horizontal and meridional convergence (differential at the west and east boundary, or the south and north boundary of the Nino3.4 region) of temperature flux respectively, and WTT_{100m} is the vertical temperature flux at the 100m depth. Prime represents the interannual anomalies (1). The residual term includes tendencies from the diffusive temperature fluxes and fluxes from the subgrid scale.

During the first three months, the positive interannual temperature tendency (Fig. 3a, red), which is contributing to the warm spikes seen in Fig.1a, can be well explained by the first four terms on the right hand side of the tendency equation. (In Fig. 3a, the sum of the four terms is represented by the black dashed line). Both the vertical temperature flux at the bottom of the layer (purple, Fig. 3a) and the meridional temperature flux convergence (green, Fig. 3a) make positive contributions to the positive temperature tendency anomalies during the 1955-1975 start years, which are partially compensated by a large negative zonal temperature flux convergence (blue, Fig. 3a).

More specifically, interannual anomalies in both vertical velocity and temperature at the 100m depth contribute to the anomalously large WTT'_{100m} during 1955-1975 in each of the first three months (not shown). Although we don't have reliable ocean observations to quantify the observed decadal change in the equatorial upwelling velocities, the domain averaged vertical velocity at 100m depth in the Nino3.4 region in Month 1 of the hindcasts is significantly higher (at the 99% confidence level) during the first two decades (1955-1974) compared to the last two decades (1995-2014), with the 20-year mean equal to 0.51 m/day and 0.38 m/day, respectively.
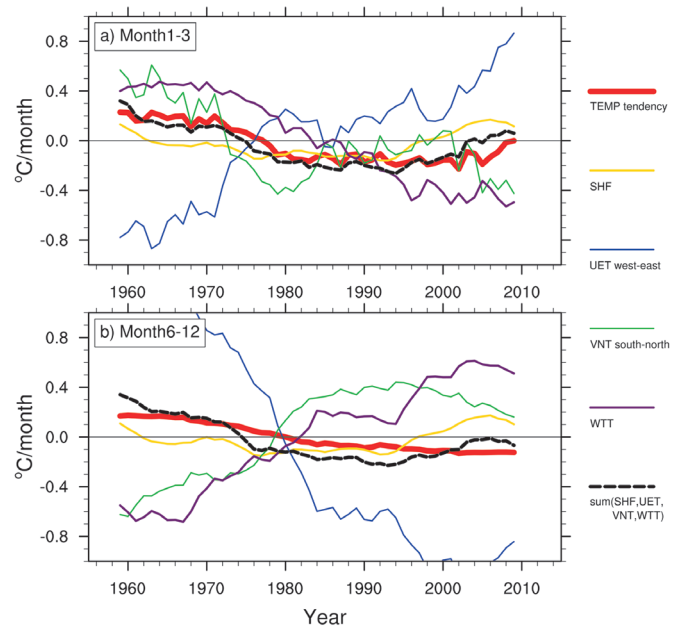

Figure 3: Budget analysis for the mixed layer temperature tendency anomalies in the Nino3.4 region averaged in a) Month1-3 and b) Month 6-12 hindcasts. All terms are shown as interannual anomalies, including temperature tendency (red), surface flux (orange), horizontal (UET, blue) and meridional (VNT, green) convergence of temperature flux, temperature flux at the 100m depth (WTT, purple), and sum of SHF, UET, VNT and WTT (black dashed). All curves are smoothed by the 10-year running averages.

Meanwhile, the corresponding 100m depth temperature during the two periods is 25.0°C and 24.2°C, respectively; the former period is significantly warmer at the 98% confidence level than the later period.

Once the warm subsurface temperature anomalies are advected into the mixed layer and the surface warming is fully established for all start years during 1955-1975 by Month 6 (not shown), the mixed layer warming is further amplified through atmosphere-ocean coupling. This is indicated by the Month 6-12 anomalous temperature tendency during 1955-1975 being mainly produced by the UET'_{w-E} term, which is partially compensated by the other four terms on the right hand side of the temperature tendency equation (Fig. 3b). Positive UET'_{w-E} is expected from westerly wind anomalies induced by the warm SST anomalies, and in a figure not shown we find the climatological zonal temperature gradient advected by the anomalous zonal current can explain a large portion of the positive temperature tendency anomalies during 1955-1975 (red, Fig. 3b). Associated with westerly surface wind anomalies are equatorial downwelling anomalies and meridional temperature divergence which make WTT'_{100m} and VNT'_{S-N} negative.

While the budget analysis can explain how the warm spikes in the pre-1975 hindcasts are triggered and

amplified, it does not single out which atmospheric forcing from the NCEP/NCAR reanalysis has played a key role in producing these ocean initial conditions. Among more than a dozen models that participated in the CMIP5 decadal prediction experiments (Kirtman et al., 2013), the Max Planck Institute Earth System Model (MPI-ESM) has a similar initial shock problem to that found in CCSM4. Their ocean initial conditions were also produced by forcing the ocean-only model with the NCEP/NCAR reanalysis. Pohlmann et al. (2016) further pin down the origins of the shock in this model to a spurious change in the NCEP/NCAR surface wind stress over 150°W-120°W, 10°S-10°N, which is strongly westward before the 1970s and eastward after 1980 compared to other reanalyses. The anomalous trade wind trend in the NCEP/NCAR reanalysis may help to explain the CCSM4 initialization shock because: a) through Ekman transport, the anomalously strong equatorial trade wind stress before the 1970s in the NCEP/NCAR reanalysis can directly induce anomalous equatorial upwelling in the CCSM4 initial states; b) in an investigation at NCAR parallel to that done at MPI, a new set of decadal prediction experiments were produced from an ocean state reconstruction generated using a different wind field (20th Century Reanalysis, Compo et al. 2006) than the prior CORE-II simulation. We find no spurious pre-1975 subsurface warming in the new ocean initial conditions. Therefore, it is likely that those especially warm subsurface initial conditions pre-1975 in CCSM4 are also caused by the NCEP/NCAR spurious wind stress. More importantly, our preliminary analysis of new hindcast experiments initialized from the ocean states produced by the 20th Century Reanalysis winds indicates no big initialization shock.

Impacts on the IPO hindcast
One might hope the model can adjust quickly to the initialization shock in the equatorial Pacific so that for the near-term forecast range (e.g. 3-5 years) it is still possible to harvest some skill from modes or patterns that have long predictability. Indeed, the CCSM4 experiments show considerable skill in predicting North Atlantic upper-ocean heat content and surface temperature up to a decade in advance (Yeager et al., 2012; Karspeck et al., 2015), which is consistent with other models' CMIP5 near-term climate predictions (Doblas-Reyes et al., 2013; Kirtman et al., 2013). There also is skill in hindcast simulations of the IPO SST pattern in terms of model anomalies computed from observations (Meehl et al., 2014; Meehl et al., 2016). However, also consistent with other models, Fig. 1d indicates prediction skill is low in the year 3-5 equatorial Pacific SST in CCSM4, raising the issue of how hindcast skill is evaluated for the Interdecadal Pacific Oscillation (IPO) (Power et al., 1999) on the near-term time scales.

The observed IPO pattern is often defined as the second empirical orthogonal function (EOF) of low-pass filtered

Pacific SSTs at 40°S-60°N, 120°E-70°W (Fig. 4a). While the spatial pattern closely resembles the El Nino composite (Zhang et al., 1997), the IPO time series has much lower frequency. It shows a negative-to-positive transition in the mid 1970s, and a positive-to-negative transition in the late 1990s and early 2000s (black line in Figs. 4de). The latter has been regarded as the main cause for the recent slow-down in observed global warming (Easterling and Wehner, 2009, Meehl et al., 2011, 2013). Motivated by the IPO's strong impact on global climate, and by the fact that it contains a midlatitude component (the Pacific Decadal Oscillation, PDO) (Mantua et al., 1997) that is more predictable than the tropical SSTs (Teng and Branstator, 2011; Branstator and Teng, 2010, 2012; Branstator et al., 2011), predicting the IPO has become a goal for the decadal prediction efforts.
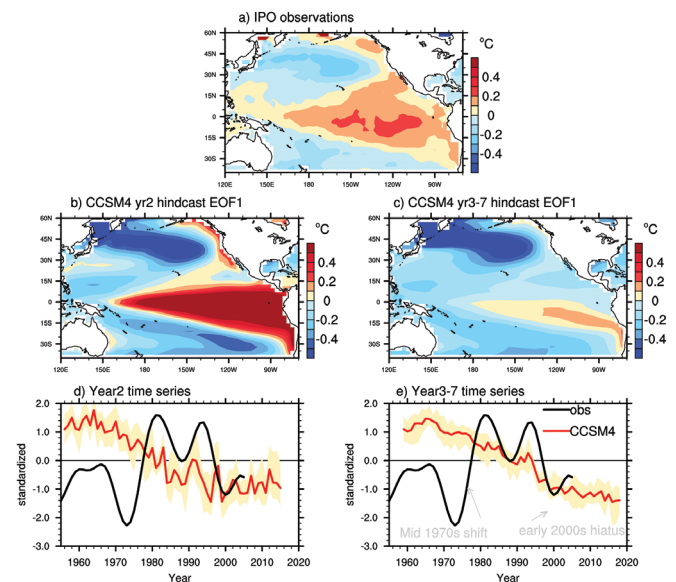

Figure 4: (a) The observed IPO: SST anomalies regressed upon the IPO index (second EOF of 10-year low-pass filtered HadISST during 1870-2016, time series shown as the black line in **(d)** and **(e)**. **(b)** and **(c)** regressed EOF1 SST anomalies from CCSM4 Year 2 (b) and Year3-7 (c) hindcasts and the corresponding time series are represented by red thick line (ensemble mean) and orange shading (spread) in d) and e).

The initialization shock has an impact on Year 2 hindcasts of the IPO in CCSM4. This is shown by an EOF analysis of the Year 2 annual mean SST anomalies over the Pacific Ocean from all start years and all ensemble members. The time series of EOF1 (ensemble average and spread is shown by the red thick line and orange shading in Fig. 4d respectively, and it accounts for 54% of the total variance) shows a downward trend, crossing from positive to negative near year 1980. While both the timing of the cross-over from positive to negative (Fig. 4d) and the amplitude of the regressed SST anomalies (Fig. 4b) in the Nino3.4 region resemble the time series of the Year 2 Nino3.4 interannual anomalies shown in Fig. 1c, the regressed SST anomalies (Fig. 4b)

trend, crossing from positive to negative near year 1980. While both the timing of the cross-over from positive to negative (Fig. 4d) and the amplitude of the regressed SST anomalies (Fig. 4b) in the Nino3.4 region resemble the time series of the Year 2 Nino3.4 interannual anomalies shown in Fig. 1c, the regressed SST anomalies (Fig. 4b) further demonstrate that the equatorial SST shock is associated mainly with a trend in the PC time series with a basin-wide IPO-like (or ENSO-like) pattern. Since we don't find such large cold temperature anomalies in the mixed layer temperature along the Kuroshio extension region in the Month1 hindcasts from 1955-1970, these cold anomalies are likely induced by the initialization shock in the equatorial Pacific through atmospheric teleconnections.

We repeat the EOF analysis for the Year 3-7 annual mean SST anomalies (Figs. 4c and e) and the PC1 also represents a downward trend and a somewhat different timing of the positive to negative change compared to Year 2, with the change occurring somewhat later around 1990-95 (Fig. 4e). This could be due to multi-year smoothing and the longer hindcast range (since the x-axis represents the central prediction year of the five year average range rather than initialization year, e.g. a hindcast for 1986-1990 is represented on the plot as 1988 and was initialized in 1984). At this longer range, the SST anomalies associated with EOF1, representing the trend in the initialized hindcasts, have damped greatly in the equatorial Pacific, but almost no damping is found in the SST anomalies in the North Pacific, possibly due to long persistence resulting from a deeper mixed layer. Thus, despite the fast adjustment in the tropical Pacific, the initialization shock represented by a trend that in some ways resembles an IPO/PDO pattern may persist in the higher latitude oceans. Thus, while the high persistence of midlatitude anomalies has the potential to give longer predictability to anomalies present in the midlatitude initial conditions, it may also degrade predictive skill as it enhances the persistence of anomalies produced by initialization shock.

Our results and those in other investigations (Sanchez-Gomez et al., 2016; Pohlmann et al., 2016) indicate that initialization shock can degrade forecasts and sometimes even produce negative skill. For example, when trying to predict the negative IPO prior to the mid-1970s, the initialization shock shown as a trend in EOF1 of both the Year 2 and Year 3-7 interannual anomalies (Figs. 4d,e) suggests the initial shock would contribute to positive values of the IPO for that time period. Therefore, skill in the positive IPO SST pattern in the CCSM4 hindcasts for this time period relative to observations (Meehl et al., 2014; 2016) could conceivably have been higher if positive values of the initialization shock trend were taken into account. There are also occasions such as in the 1990s when the trends in the Year 3-7 anomalies, which to a large extent may be caused by the initialization shock, are

in phase with the observed IPO such that those negative trend values could artificially contribute some skill in hindcasts for the negative phase of the IPO. A better understating of the time-dependent characterization of initialization shock in CCSM4 is thus necessary in order to correctly interpret the model skill.

References
Branstator, G. and H. Teng, 2010: Two limits of initial-value decadal predictability in a CGCM. J. Climate, 23, 6292-6311.

Branstator, G. and coauthors, 2011: Systematic estimates of initial-value decadal predictability for six AOGCMs. J. Climate, 25, 1827-1846.

Branstator, G. and H. Teng, 2012: Potential impact of initialization on decadal predictions as assessed for CMIP5 models. Geophys. Res. Lett., doi:10.1029/2012GL051974

Compo, G. P., J. S. Whitaker, and P. D. Sardeshmukh, 2006: Feasibility of a 100-year reanalysis using only surface pressure data. Bull. Am. Meteorol. Soc., 87, 175-190.

CLIVAR, 2011: Data and bias correction for decadal climate prediction. CLIVAR Publication Series 150, International CLIVAR Project Office, 4pp.

Danabasoglu, G. and coauthors, 2014: North Atlantic simulations in coordinated ocean-ice reference experiments phase II (CORE-II). Part I: mean states. Ocean Modelling, 73, 76-107.

Doblas-Reyes F. J. and coauthors, 2013: Initialized near-term regional climate change prediction. Nature Comms, doi:10.1038/ncomms2704

Easterling, D. R., and M. F. Wehner, 2009: Is the climate warming or cooling? Geophys. Res. Lett., 36, doi:10.1029/2009GL037810.

Gent, P. and coauthors, 2011: The Community Climate System Model version 4. J. Climate, 24, 4973-4991.

Kalnay, E and coauthors, 1996: The NCEP/NCAR 40-year reanalysis project. Bull. Am. Meteorol. Soc., 77, 437-471.

Karspeck, A. and coauthors, 2015: An evaluation of experimental decadal predictions using CCSM4, Climate Dyn, 44, 907-923.

Kirtman, B. and coauthors, 2013: Near-term climate change: projections and predictions. In: Stocker T.F. et al. (eds) Climate Change 2013: the physical science basis, contribution of working group 1 to the fifth assessment report of the intergovernmental panel on climate change, Cambridge University Press, Cambridge, pp 953-1028.

Kosaka, Y. and S.-P. Xie, 2013: Recent global-warming hiatus tied to equatorial Pacific surface cooling. Nature, 501, 403-407.

Levitus, S. and coauthors, 2009: Global ocean heat content 1955-2008 in light of recently revealed instrumentation problem. Geophys. Res. Lett., doi: 10.1029/2008GL037155

Mantua, N. J and coauthors, 1997: A Pacific Interdecadal Climate Oscillation with impacts on salmon production. Bull. Amer. Meteor. Soc., 78, 1069–1079.

Meehl, G. A. and coauthors, 2011: Model-based evidence of deep-ocean heat uptake during surface-temperature hiatus periods. Nat. Climate Change, 1, 360-364.

Meehl G. A. and coauthors, 2013: Externally forced and internally generated decadal climate variability associated with the Interdecadal Pacific Oscillation. J. Climate, 26, 7298-7310.

Meehl G. A. and H. Teng, 2012: Case studies for initialized decadal hindcasts and predictions for the Pacific region. Geophys. Res. Lett., doi: 10.1029/2012GL053423.

Meehl, G. A. and coauthors, 2014a: Decadal climate prediction: an update from the trenches. Bull. Am. Meteorol. Soc., 95, 243-267.

Meehl, G. A., H. Teng, and J. M. Arblaster, 2014b: Climate model simulations of the observed early-2000s hiatus of global warming. Nat. Climate Change, 4, 898-902.

Meehl G. A. and H. Teng, 2014a: CMIP5 multi-model hindcasts for the mid-1970s shift and early 2000s hiatus and predictions for 2016-2035. Geophys. Res. Lett., doi: 10.1002/2014GL059256.

Meehl G. A. and H. Teng, 2014b: regional precipitation simulations for the mid-1970s shift and early-2000s hiatus. Geophys. Res. Lett., doi: 10.1102/2014GL061778.

Meehl, G. A., A. Hu and H. Teng, 2016: Initialized decadal prediction for transition to positive phase of the Interdecadal Pacific Oscillation. Nature Comm, doi: 10.1038/ncomms11718.

Pohlmann, H. and coauthors, 2016: Initialization shock in decadal hindcasts due to errors in wind stress over the tropical Pacific. Clim Dyn, doi: 10.1007/s00382-016-3486-8.

Power, S. and coauthors, 1999: Interdecadal modulation of the impact of ENSO on Australia. Climate. Dyn., 15, 319-324.

Rayner, N. A. and coauthors, 2003: Global analysis of sea surface temperature, sea ice, and night marine air temperature since the late nineteenth century. J. Geophys. Res., 108:4407, doi: 10.1029/2002JD002670.

Sanchez-Gomez, E. and coauthors, 2016: Drift dynamics in a coupled model initialized for decadal forecasts. Climate Dyn., 46, 1819-1840.

Teng H. and G. Branstator, 2011: Initial-value predictability of prominent modes of North Pacific subsurface temperature in a CGCM, J. Climate, 36, 1813-1834.

Taylor, K.E., R.J. Stouffer and G.A. Meehl, 2012: An overview of CMIP5 and the experiment design. Bull Am Meteorol Soc, 93, 485-498.

Yeager, S, and coauthors, 2012: A decadal prediction case study: late twentieth-century North Atlantic ocean heat content. J. Climate, 25, 5173-5189.

Zhang, Y., J. M. Wallace, and D. S. Battisti, 1997: ENSO-like interdecadal variability: 1900-1993. J. Climate, 10, 1004-1020.